HAWC — a far-infrared camera for SOFIA

D. A. Harper,[a] C. Allen,[b] M. Amato,[b] T. Ames,[b] A. Bartels,[b] S. Casey,[c]
R. Derro,[b] Rh. Evans,[a] I. Gatley,[d] S. Heimsath,[a] A. Hermida,[b] M. Jhabvala,[b]
J. Kastner,[d] R. F. Loewenstein,[a] S. H. Moseley,[b] R. J. Pernic,[a] T. Rennick,[a] H. Rhody,[d]
D. Sandford,[a] R. Shafer,[b] P. Shirron,[b] G. Voellmer,[b] S. Wang,[a] and J. Wirth[a]

[a]University of Chicago, Chicago, IL 60637 USA
[b]NASA Goddard Space Flight Center, Greenbelt, MD 20771 USA
[c]USRA-SOFIA, Moffett Field, CA 94035-1000 USA
[d]Center for Imaging Science, Rochester Institute of Technology,
Rochester, NY 14623-5603 USA

ABSTRACT

When SOFIA enters operation, it will be the largest far-infrared telescope available, so it will have the best intrinsic angular resolution. HAWC (High-resolution Airborne Wideband Camera) is a far-infrared camera designed to cover the 40–300 micron spectral range at the highest possible angular resolution. Its purpose is to provide a sensitive, versatile, and reliable facility-imaging capability for SOFIA's user community during its first operational years.

HAWC will utilize a 12×32 pixel array of bolometer detectors constructed using the ion-implanted silicon pop-up detector technology being developed at Goddard Space Flight Center. This new technology enables construction of close-packed, two-dimensional arrays of bolometers with high quantum efficiency and area filling factors of greater than 95%. The array will be cooled by an adiabatic demagnetization refrigerator and operated at a temperature of 0.2 K.

HAWC data processing software will be developed within the context of an Observatory-wide "data-cycle system" which will provide an integrated environment for proposal preparation, flight planning, data processing, calibration, analysis, and archiving.

Keywords: data pipeline, detectors, bolometer, far-infrared, SOFIA, XML

1. INTRODUCTION

SOFIA (Stratospheric Observatory for Infrared Astronomy) and SIRTF (Space Infrared Telescope Facility) will provide the astronomy community's principal access to the far-infrared spectral region during most of the coming decade. SOFIA is a 2.5 m telescope mounted in an aircraft. It will support an evolving array of facility and principal-investigator instruments. SIRTF is a cryogenic telescope with a fixed instrument complement composed of broadband imagers and low-resolution spectrometers. SIRTF's low thermal background will give it unsurpassed sensitivity for those spatial frequencies to which it is sensitive. SOFIA's large aperture will provide access to spatial frequencies $\geq 0.8/\lambda(\mathrm{m})$, where SIRTF has no sensitivity, and its instrument complement will include a variety of high-resolution spectrometers. HAWC (High-resolution Airborne Wideband Camera) is a camera with four broadband ($2.5<R<10$) filters which span the far-infrared ($40 - 300$ μm), a part of the spectrum which is inaccessible from ground-based observatories. It is one of four instruments selected as first-light facility instruments for SOFIA. The others include FLITECAM, a near-infrared camera/spectrometer; FORCAST, a mid-infrared multiband imager; and AIRES, a far-infrared spectrometer (for additional information on SOFIA instruments, see the SOFIA website at http://www.sofia.usra.edu/).

As a facility instrument, HAWC will be employed for a wide variety of observations. Some of the scientific questions it is expected to address include:

- The formation of stars and stellar clusters within our Galaxy;
- Star formation in external galaxies;
- Structure and evolution of protoplanetary and remnant disks;

- The return of gas and dust to the interstellar medium from stars;
- The composition and life-cycle of interstellar dust;
- The interactions between young stars and their environments;
- Conditions in regions surrounding active galactic nuclei.

In these processes, much of the optical and ultraviolet light generated by primary energy sources such as stars or accretion disks may be locally absorbed by interstellar dust and re-radiated in the infrared. Often, half or more of the total flux emerges beyond 40 μm, and many of the emitting regions have complex geometries and/or multiple sources of heating. Far-infrared observations at the highest possible angular resolution are essential for understanding their structure and energetics.

2. INSTRUMENT OVERVIEW

The most important drivers for HAWC's design are directly linked to its primary objective — far-infrared imaging at the highest angular resolution possible with the SOFIA telescope. They include the following. (1) HAWC must be able to cover the 40 – 300 μm spectral region which is inaccessible to ground-based telescopes. (2) The filter bandwidths need to be narrow enough to limit the color dependence of the instrumental point spread function, effective wavelength, and mean transmission. (3) The spectral bands should be matched to regions with high atmospheric transmission to maximize the ratio of signal to noise and minimize the effects of variable extinction. (4) Achieving diffraction-limited performance across the entire spectral range requires matching the detector pixel scale to the size of the Airy disk at each wavelength. (5) The instrument must operate sensitively, efficiently, and reliably in its unique airborne environment.

The principal features of the instrument are shown in Figure 1. The light from the telescope enters from the right and reflects at an acute angle from a flat mirror before coming to a focus. The diverging beam then reflects from a field mirror which re-images the telescope entrance pupil onto a helium-temperature pupil within the instrument's cryostat. The light entering the cold pupil is focused onto a 12×32 pixel array of ion-implanted silicon bolometers by one of four lenses with focal lengths chosen to match the pixel size to the diffraction limit at wavelengths of 58, 90, 155, and 215 μm. Spectral filtering is accomplished by a short-wavelength blocking filter in front of the cold pupil and bandpass filters mounted with the corresponding lenses. There are two principal mechanisms. The first can interchange pupil masks or auxiliary filters in the plane of the cold pupil. The second is a carousel which switches the re-imaging lenses.

The detector array is cooled to a temperature of 0.2 K by a single-stage adiabatic demagnetization refrigerator (ADR). The base operating temperature of the ADR is maintained at 4 K by a large liquid helium reservoir. Secondary cooling for the liquid helium cryostat is provided by two vapor-cooled radiation shields.

Signals from each of the 384 high-impedance bolometers pass through unity-gain JFET preamplifiers rigidly integrated with the detector array assembly. They are further amplified and digitized by a set of warm electronics mounted on the vacuum shell of the cryostat, then transmitted through a fiber-optic cable from the telescope to a data acquisition computer mounted in a rack attached to the cabin floor of the aircraft.

In the following sections, we describe HAWC's major subsystems and design features in greater detail. The instrument's optical specifications and predicted sensitivities are summarized in Table 1.

3. SPECTRAL PASSBANDS

To address its scientific objectives, HAWC must be able to efficiently characterize the spectral energy distribution of the large-grain component of interstellar dust — the principal source of 40–300 μm continuum emission from astronomical sources. Unlike the non-equilibrium emission from very small grains and macromolecules, which dominates at near- and mid-infrared wavelengths and which is marked by prominent emission bands, the far-infrared continuum is relatively smooth and featureless; the character of the spectral energy distribution is governed not by the composition of the dust but by the grain temperatures and number densities present along each line of sight. Images in four filter passbands will provide a reliable basis for inferring the spatial distribution, temperatures, and column densities of the large grains.

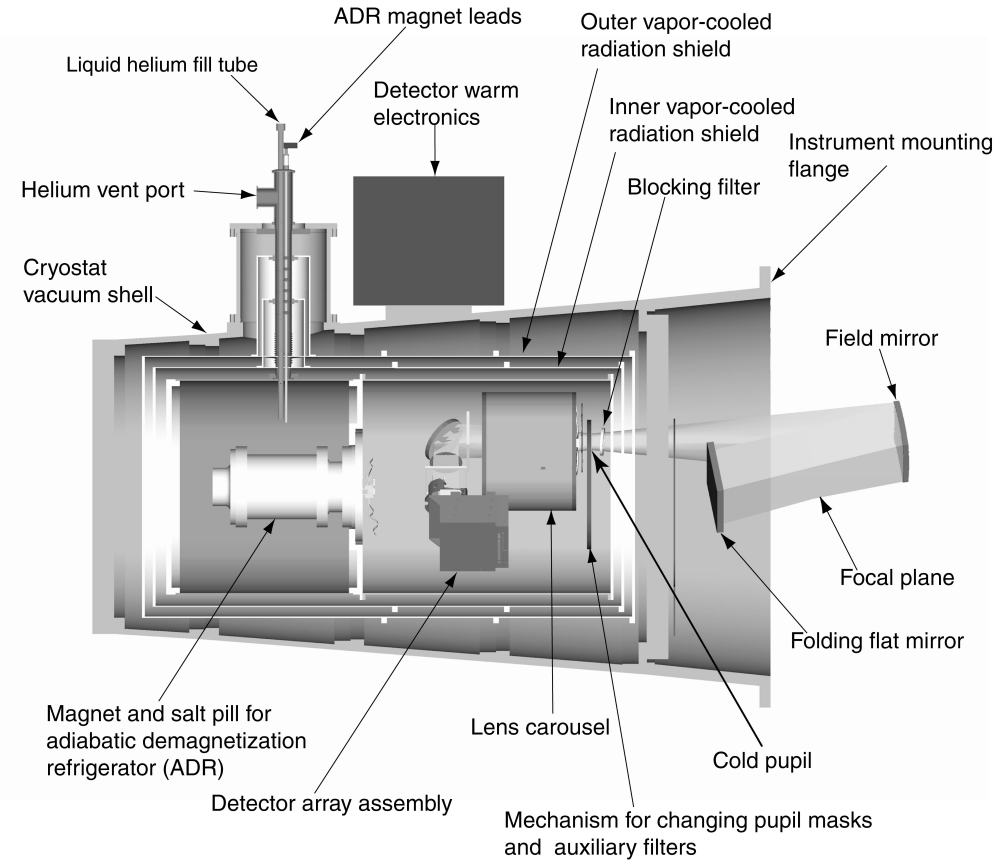

Figure 1. Physical layout of the HAWC instrument.

Table 1: HAWC Optical and Photometric Specifications

	Units	Band 1	Band 2	Band 3	Band 4
Central wavelength	μm	58	90	155	215
Bandwidth	$\Delta\lambda/\lambda$	0.23	0.1	0.2	0.23
Pixel size	arcsec	2.25	3.50	6.00	8.00
Image diameter (FWHM)	arcsec	6	9	16	22
Detector array field size	arcsec	27×72	42×112	72×192	96×256
Detector array areal filling factor	%	>95	>95	>95	>95
Mean transmission (cold optics)	%	0.14	0.18	0.22	0.22
Mean transmission (warm optics plus vacuum window)	%	0.51	0.63	0.69	0.70
Mean transmission (atmosphere, 10 μm H_2O, 40° elevation)	%	0.67	0.73	0.63	0.82
Background power per pixel	nW	0.061	0.023	0.039	0.022
NEP (thermal background limit, one pixel)	fW/Hz$^{1/2}$	0.66	0.34	0.35	0.23
Frequency range (for background-limited performance)	Hz	$5-100$	$5-100$	$5-100$	$5-100$
NEFD (1σ, background limit, $A\Omega = \lambda^2$)	Jy/Hz$^{1/2}$	1.3	1.3	1.0	0.7
NEFD (1σ, background limit, $A\Omega = \lambda^2$)	mJy(1 hr)	15.0	15.0	12.0	7.8

To help determine the optimal filter characteristics for HAWC, we have calculated mean atmospheric transmission and noise equivalent flux density for ranges of effective wavelength, bandwidth, atmospheric water vapor, and source spectrum. For filter bandwidths small enough ($\Delta\lambda/\lambda \lesssim 0.25$) to avoid excessive sensitivity to source color, there are distinct peaks in measurement speed corresponding to regions of particularly good atmospheric transmission. The positions of the peaks are relatively insensitive to the assumed source spectrum. Based on these results, we have selected four bands with the characteristics shown in Figure 2 and described in Table 1.

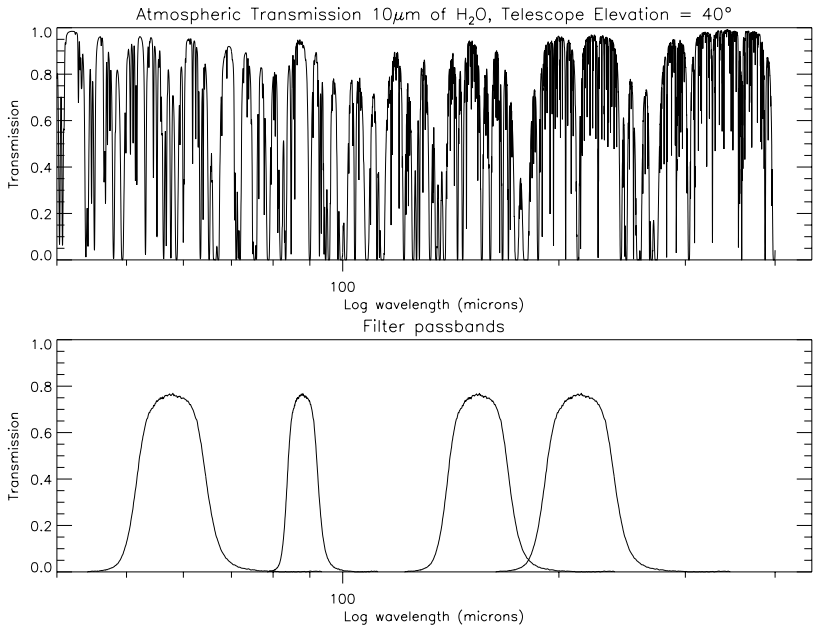

Figure 2. Spectral passbands and atmospheric transmission (computed for 10 μm of precipitable water and a telescope elevation angle of 40°).

4. OPTICS

The goals of HAWC's optical design are to achieve diffraction-limited imagery in all spectral bands, to maximize transmission, and to minimize thermal emission and stray light.

Our choice of optical layout is driven by the fact that the largest source of emission in the optical path is the vacuum window of the cryostat. The minimum allowable window thickness is determined by the field of view at the longest wavelength. Placing the instrument pupil near the vacuum window minimizes the diameter and thickness of the window, more than offsetting the additional thermal emission from the two mirrors in the warm fore-optics. Also, unlike a layout in which the focal plane lies near the window, this scheme allows all spectral bands to share a *common* cold pupil which can be aligned with the telescope aperture by adjusting optical elements external to the cryostat. Note that because of diffraction, the optics must accept a field which is significantly larger than the geometrical field. This is illustrated in Figure 3, which shows how the size of the field stop affects the pupil intensity distribution seen by different detectors. This type of vignetting is undesirable for two reasons. First, the edge detectors suffer decreased throughput and increased sensitivity to stray light. Second, the differences between the pupil-plane intensity patterns for different detectors within the array make compensating for "sky noise" (fluctuations in thermal background in excess of photon noise) more difficult. Observations on the Kuiper Airborne Observatory showed that such noise exists, that its magnitude can be significant with respect to photon noise, that it is highly correlated for different points within the focal plane, and that it can be reduced or eliminated using appropriate data-reduction algorithms. HAWC's optics are sized to avoid vignetting through the fifth Airy ring in Band 4 (215 μm) for detector arrays as large as 32×32 pixels.

The changes in magnification needed to match the detector pixel size to the diffraction limit in each band are effected by rotating a carousel containing four independent sets of lenses and spectral bandpass filters. This

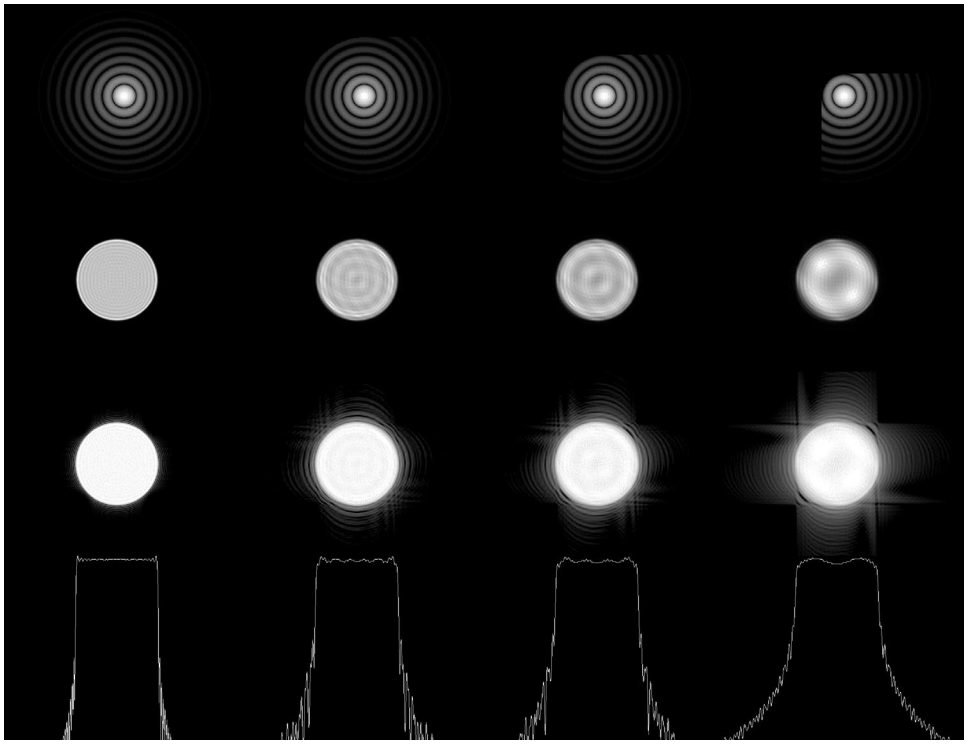

Figure 3. Field-plane (top row) and pupil-plane (below) intensity distributions for central (left column) and corner detectors (right three columns). The second through fourth columns illustrate the effects of field stops which extend beyond the geometrical field by amounts equal to the radii of the sixth, fourth, and second dark ring of the Airy function. The one-dimensional cross sections in the fourth row and the two-dimensional plots in the third show the logarithm of the intensity. All of the Airy patterns are artificially truncated beyond the ninth dark ring to limit computation time.

arrangement allows the optical characteristics of the lenses, antireflection coatings, and filters to be separately optimized for each band. The lenses for the two long-wavelength bands are singlets and those for the short-wavelength bands are doublets. All deliver diffraction-limited performance for fields at least as large as 32×32 pixels, so the instrument will be able to accommodate larger detector arrays in the future.

The lens carousel and pupil-plane filter wheel are actuated by Geneva mechanisms enhanced by the addition of spring-loaded detents. The Geneva provides reliable indexing without the need for critical positional control of the cryogenic motors. The detent gives more accurate positioning, lower backlash, and better stability than the Geneva alone. The detent arm engages V-shaped slots at the outer perimeters of the rotating assemblies. It is actuated by a cam on the Geneva shaft, reducing the motor torque required to extend the spring.

The magnifications selected for HAWC (see Table 1) represent a compromise between mapping speed and sensitivity to high spatial frequencies. The angular sizes of the pixels are slightly less than $\lambda/2D$. Larger pixels would significantly attenuate high spatial frequencies. Smaller pixels would significantly increase the number of independent pointings required to cover areas larger than the size of the array. For these pixel scales, positional dithering (subsampling) will be required to adequately sample and reconstruct the highest spatial frequencies detected by the telescope. The dithering will be an integral feature of the standard observing mode, so the full resolution of SOFIA will be preserved in all images made with HAWC.

5. DETECTOR ARRAY

The primary requirements for HAWC's detector array are diffraction-limited sampling of the focal plane, high quantum efficiency, and background-limited performance over the 40-300 μm spectral range. The design we have chosen

is a 12×32 array of ion-implanted silicon bolometers. It is being developed as part of a program now underway at Goddard Space Flight Center to produce close-packed bolometer arrays with large formats (ultimately 32×32 or larger). The specific technologies and design features incorporated in the HAWC array have been selected to provide the best possible performance when SOFIA begins operation.

The first objective, efficient spatial sampling of the focal plane at the highest possible angular resolution, is accomplished using a densely packed array of square detector elements with a geometrical filling factor of $> 95\%$. The close-packing is achieved by stacking 1×32 rows of "pop-up" detectors fabricated from 1 μm thick silicon. This is illustrated in Figure 4. The upper panel of the figure shows 32 1 mm×1 mm×1 μm detector pixels, each suspended in free space by four narrow legs. To fabricate a single 1×32 row, the silicon frame is placed in a jig, the ends of the frame to the right and left of the slot in which the detectors are suspended are removed, and the other sides of the frame are folded back and bonded to a bus bar slightly less than 1 mm thick. Thus the 32 pairs of ion-implanted electrical leads running down the detector legs to the edge of the frame are re-directed at right angles to the plane of the detectors. The key to bending the legs without breaking them is their geometry, which allows the strain associated with the right-angle bend to be distributed as a torsional flexure along a segment of the leg running parallel to the edge of the detector. The lower panels in Figure 4 show close-up images of individual pixels before and after folding and a detailed view of the leg geometry.

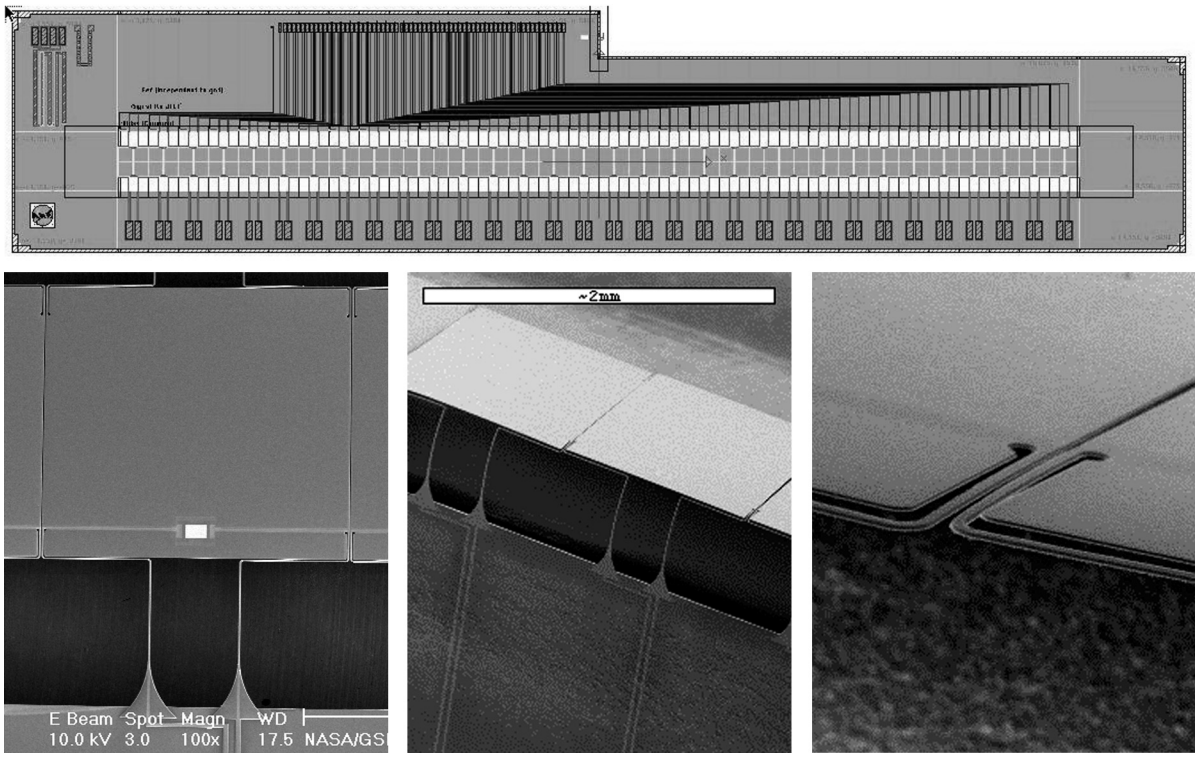

Figure 4. Pop-up detectors. The top panel shows a one-dimensional micromachined array before folding. The two lower-left panels are electron-microscope images of pop-up detector pixels before and after folding. The lower right panel shows a close-up view of the torsion flexures which make the folding possible.

Ion-implanted semiconducting thermometers have been used in many infrared and particle detection applications, in single detectors and in integrated linear arrays. Their performance has been excellent, achieving sensitivities limited only by thermodynamic fluctuations. The pop-up geometry described above solves the most crucial problem associated with extending the technology to large two-dimensional arrays. Additional challenges include coupling the signals from the high-impedance detectors to quiet amplifiers (typically individual JFETs which must be operated at temperatures of 70–120 K) and dealing with the large number of signal lines.

The primary alternative technology considered for HAWC was that of bolometers using superconducting transition

edge sensors (TESs) as thermometers. Such devices have achieved excellent performance as X-ray microcalorimeters and show great promise as far-infrared detectors. An advantage of the TES detectors is excellent performance using SQUID amplifiers. These devices operate at very low power and perform well at 4.2 K. This greatly simplifies the electrical and thermal design problem of coupling the detector signal to its front-end amplifier. Furthermore, a SQUID multiplexer has been developed (Chervenak et al. 1999) which greatly reduces the number of signal lines which must exit the cryostat, in principle bringing the same sort of multiplexing capability to the far-infrared that has created a revolution in the performance of near- and mid-infrared detectors.

We selected semiconductor thermometers for HAWC because they are a well-developed technology which has been demonstrated on the Kuiper Airborne Observatory (KAO) and on the XRS instrument for Astro-E. Because of the large cooling capacity of the HAWC cryostat, the detectors can use the same type of electronics proven on the KAO. This combination of detectors and electronics represents a low-risk path to delivery by SOFIA's first light.

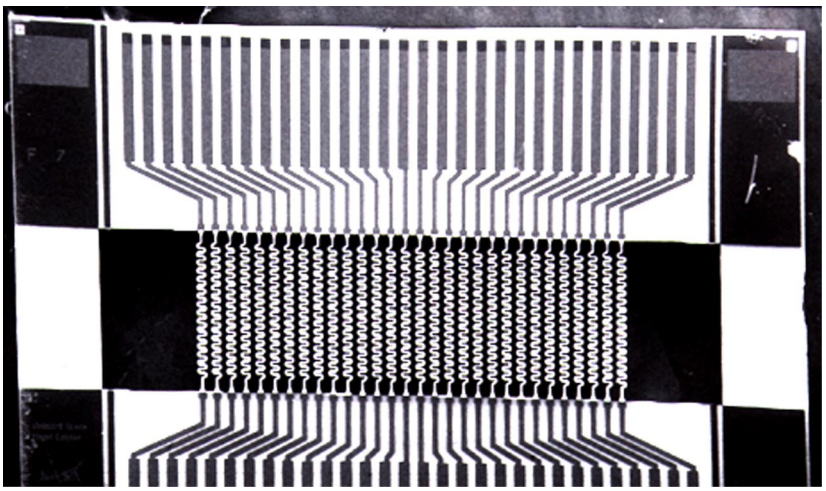

Figure 5. Microbridge thermal isolators. The serpentine traces in the center of the picture are the free-standing electrical conductors. The spacing between traces is ~ 130 μm. The white areas to the left and right of the traces are the portions of the frame which are removed after assembly.

The fabrication process for the complete detector assembly is illustrated in Figure 6. After folding, each detector/bus bar assembly is attached to a ceramic fanout card via a microbridge thermal isolator. In order to provide room for bonding the electrical leads, each bus bar/fanout card unit is paired with a unit having a complementary cutout. These pairs are assembled one by one into a supporting frame. The bus bars are attached to a 0.2 K stage which is suspended from the 4 K main frame of the detector assembly with Kevlar cords, and the fanout cards are attached to the 4 K structure. Then, the ends of the microbridge frames are removed, and the next pair of cards is added to the stack. Three 304-pin electrical connecters bonded to the fanout cards connect the detectors to three boards containing the 120 K JFET preamplifiers, which are also thermally isolated with microbridge units.

The detector must have background-limited performance and high quantum efficiency in all HAWC's photometric bands. These requirements influence the design in two ways. The bolometers' absorptive coatings must efficiently cover a wavelength range of almost three octaves, and their electrical characteristics must be chosen to accommodate the different background powers in the four bands. To address the former, we have chosen a frequency-independent absorbing film (Clark et al. 1977) which provides 50% quantum efficiency across the full wavelength range. To address the latter, we have employed the optimization approach described by Mather (1984) for ideal thermal detectors, assuming that the detector heat capacity has been minimized and the primary quantities to be optimized are the thermal conductance of the detector and the operating bias power. The background powers in the four spectral bands differ by a up to a factor of three (see Table 1). The most demanding case is the 215 μm band, for which the incident power and background-limited NEP are lowest. We have chosen to optimize the thermal performance of the detector for this band. This also produces background-limited performance for the other spectral

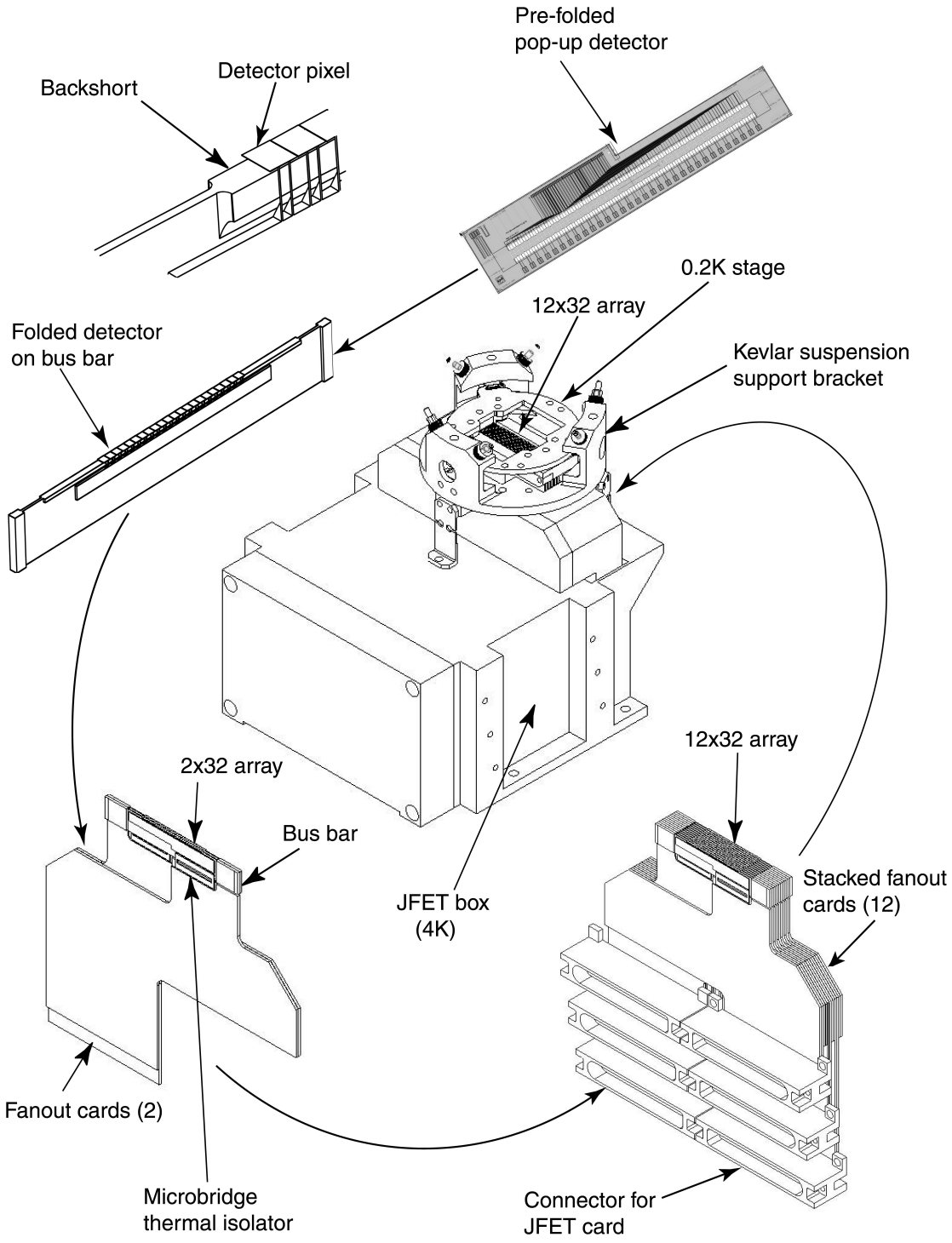

Figure 6. Schematic diagram of the fabrication process of the HAWC detector array.

bands. To assure that performance is not limited by non-ideal behavior, we have chosen a thermometer implant that covers the entire detector area. With this choice, the devices should have negligible electrical nonlinearities and current noise over their full operating range (see Han et al. 1998).

After impedance transformation by the unity-gain JFET amplifiers integrated with the detector array, analog signals for each of the 384 pixels are routed to a set of warm electronics attached to the vacuum shell of the cryostat. There, they are amplified and digitized by individual analog-to-digital converters. The digital signals are multiplexed and transmitted over an optical fiber link to a data-acquisition computer in a rack mounted to the cabin floor of the aircraft. Except for minor changes in component selection and repackaging to accommodate the larger number of data channels, the signal chain is virtually identical to 64-channel systems operated successfully on the KAO just prior to its decommissioning in 1995.

The HAWC detector development is part of a larger detector-technology initiative currently underway at Goddard Space Flight Center. Arrays of pop-up detectors with physical characteristics similar to those required for HAWC were recently built and tested in the development program for the SPIRE instrument for FIRST. The SPIRE detectors differed in thermometer technology (SPIRE used TES detectors) and thermal conductance (SPIRE had backgrounds ~ 100 times lower than HAWC), but the detector geometry and overall mechanical designs are similar. The SPIRE detectors used an absorbing film and resonant backshort designed to give a narrow-band absorption of 100%, but the film composition and deposition process is the same as planned for the HAWC broadband coating.

The SPIRE prototype testing validated several key aspects of detector design relevant to HAWC. Both the SPIRE prototype and the HAWC design use a kinematic structure of pre-tensioned Kevlar cords to support and thermally isolate the detectors. The stiffness and thermal conductance of the Kevlar suspension agreed with predictions. Also, the electrical connections between the SPIRE detectors (T = 0.3 K) and readout electronics (T = 1.5 K) were made using plated, micromachined Si microbridge interconnects similar to those which will be used to isolate the 0.2 K and 120 K stages in the HAWC detector assembly.

The SPIRE work also validated several of the manufacturing processes to be used for the HAWC arrays. The lithographic and micromachining processes used to manufacture the SPIRE detectors yielded very reproduceable results. Their properties could be precisely controlled, and devices which had similar mechanical properties had similar thermal properties. The performance of the metallic absorbing film was also consistent with predictions. The optical efficiency of the detectors was measured to be $\gtrsim$90%.

6. CRYOGENICS

The primary design requirements for HAWC's cryogenic system are (1) to assure background-limited detector performance, (2) to minimize mechanical deflections caused by aircraft motions, vibrations, or changes in orientation, and (3) to operate simply, efficiently, and reliably as a facility instrument.

The primary cooling for the adiabatic demagnetization refrigerator (ADR) and cold optics subsystem will be provided by a vapor-cooled He^4 cryostat similar in design to two long-hold-time systems developed for use at the South Pole. The dual vapor-cooled shields assure good cryogenic performance without the need for liquid nitrogen. The helium reservoir and cold optics subassembly are thermally isolated and kinematically positioned by Kevlar straps.

We have selected an ADR to cool the HAWC detector array because of its simplicity of operation, lack of moving parts, and ability to operate over a wide temperature range, including temperatures much lower than the nominal detector operating temperature of 0.2 K. The design chosen requires only one stage to reach the desired operating temperature from the relatively warm (4 K) heat sink.

The ADR is based on the design developed for the X-Ray Spectrometer (XRS) built for the ASTRO-E satellite mission. The XRS refrigerator was designed to operate at 60 mK. It used a ferric ammonium alum (FAA) salt pill, a 2 Tesla magnet, a He^3 gas-gap heat switch, and a Kevlar thermal isolation system. In many respects, the HAWC requirements are more easily met than those of XRS. At the higher operating temperature, the paramagnetic salt has a significantly larger cooling power per unit mass, and the relaxed requirements on the time to recycle the system and the amount of heat rejected to the helium bath allow parasitic heat loads to be greatly reduced. As a result, the XRS design gives large performance margins for HAWC. The only significant change is the size of the superconducting magnet. The use of a 4 K heat sink requires a much larger magnetic field for HAWC than for XRS. However, the requirement (at least 5 T) can be satisfied by a commercially available, off-the-shelf magnet. To further increase

performance, we have taken advantage of HAWC's less stringent vibrational requirements and larger available space by redesigning the suspension system to move the heat switch out of the structural load path. We have also reduced the parasitic thermal conductance of the heat switch.

The mechanical design of the system is dominated by the need to keep its resonant frequencies above ∼150 Hz. This requirement is derived from analytical predictions of accelerations caused by turbulent aerodynamic loads on the telescope, which indicate that the highest significant resonant frequencies lie at ∼120 Hz. Meeting this criterion also assures that deflections due to aircraft motion and changes in telescope orientation have a negligible effect on pointing accuracy. The conical shell of the cryostat is the most efficient shape for maximizing resonant frequency and minimizing instrument weight. The Kevlar suspension straps simultaneously meet the requirements for mechanical stiffness and cryogenic isolation. A thermal model verified by performance tests of the South Pole cryostats predicts He^4 hold times of ≥24 hr in operational mode and ∼3 days in standby mode. A model based on experimental tests of XRS predicts ADR set-up and hold times of ≤2 hr and ≥16 hr, respectively.

7. SOFTWARE

The HAWC Instrument Control and Data Acquisition software takes advantage of the NASA Goddard Space Flight Center's Instrument Remote Control (IRC) project (Ames et al. 2000). The IRC creates an extensible framework, which may be used to generate platform-independent software (in the JAVA language) for a wide variety of instruments. Instruments are described in the Instrument Markup Language (IML), a vocabulary based on a W3C standard, the Extensible Markup Language (XML). This description provides information on graphical user interfaces (GUIs), communication protocols, command formats, data streams, and data processing algorithms — in short, all the information needed for the framework to generate instrument-specific software.

Some of the beneficial attributes of the design are:

- A clearly defined interface between hardware and software;
- Dynamic instrument configuration and control (change the description and see the immediate results);
- An object-oriented component architecture that supports dynamic instrument configuration and control;
- The capability of capturing a detailed description of an instrument via a markup language (an extension of XML);
- The capability of producing a large portion of the documentation automatically from the description;
- Platform independence for remote instrument control, monitoring, and acquisition of science data.

The HAWC software accesses a library of visualizations, which may be expanded with additional components. Examples are a 12×32 strip chart and a 12×32 real-time imager. The GUIs are designed to present a consistent "look and feel." Information is presented in a hierarchical structure that permits easy navigation from higher level data abstractions to lower level details. Whenever possible, data are mapped to graphical representations of the physical or logical instrument components. The user will be able to modify how data are presented.

In addition to the 384 bolometer channels, the data stream will have an additional 32 status channels, two of which will hold the digitized waveforms of the two-axis oscillating secondary mirror. The total bandwidth for these data will be between 1.664 and 6.656 MB s^{-1}, assuming 4 byte words and a sample rate between 1 and 4 kHz. Depending on the type of chopping, various demodulation algorithms may be needed. Like all HAWC data-reduction software, these algorithms will be modular and easily plugged into the system as necessary.

The data processing pipeline is designed to operate automatically, with little or no interaction from the user. Quick-look data will be available during the observation, with a completed mosaic image delivered within several minutes after the observation leg is completed. Streaming and disk-archived data will be processed both during and after flights. Like visualizations, the modular reduction packages are plugged into the HAWC software as components. The HAWC data processing software is being developed within the context of an Observatory-wide "data-cycle system" which will provide an integrated environment for proposal preparation, flight planning, data processing, calibration, analysis, and archiving.

ACKNOWLEDGMENTS

This work was supported by NASA under grant USRA 8500-98 407.

REFERENCES

Ames, T., Koons, L., Sall, K., and Warsaw, C. 2000, "Using XML and Java for telescope and instrumentation control," in *SPIE Proceedings, Astronomical Telescopes and Instrumentation 2000.*

Chervenak, J. A., Irwin, K. D., Grossman, E. N., Martinis, J. M., Reintsema, C. D., and Huber, M. E. 1999, "Superconducting multiplexer for arrays of transition edge sensors," *Appl. Phys. Lett.,* **74,** 4043-4045.

Clarke, J., Hoffer, G. I., Richards, P. L., and Yeh, N.-H. 1977, "Superconductive bolometers for submillimeter wavelengths," *J. Appl. Phys.,* **48**, 4865-4879.

Han, S. I., et al. 1998, "Intrinsic 1/f noise in doped silicon thermistors for cryogenic calorimeters," in *SPIE Proceedings, EUV, X-Ray, and Gamma-Ray Instrumentation for Astronomy IX*, **3445**, 640-644.

Mather, J. 1984, "Bolometers: ultimate sensitivity, optimization, and amplifier coupling," *Appl. Optics*, **23**, 584-588.